Vol. 38, No. 1
March 2020

JOURNAL OF
RADIATION
EFFECTS
Research and Engineering

Displacement Damage Effects in Germanium Tin LEDs

K. Choe, M.R. Hogsed, N. Miguel, J.W. McClory, and J. Kouvetakis

This paper was presented at the 36th Annual HEART Conference
San Diego, CA, April 8–12, 2019.

Prepared by Amentum for the HEART Society under contract to NSWC Crane

This work was sponsored by the Air Force Office of Scientific Research (11767875-AFIT and FA9550–17–1–0314-ASU).

JOURNAL OF RADIATION EFFECTS,
Research and Engineering
Vol. 38, No. 1, March 2020

DISPLACEMENT DAMAGE EFFECTS IN GERMANIUM TIN LEDS

K. Choe, M.R. Hogsed, N. Miguel, and J.W. McClory
Air Force Institute of Technology
Wright-Patterson AFB, OH

J. Kouvetakis
Arizona State University
Tempe, AZ

Abstract

The effects of radiation-induced deep-level defects on the electroluminescence intensity produced by $Ge_{1-x}Sn_x$-based light emitting diodes (LEDs) are studied as a function of varying tin concentrations (x = 0, 0.02, 0.069, and 0.094). All of these devices tolerate relatively high levels of proton displacement damage, and devices with higher Sn concentration are up to 10 times more tolerant of displacement damage than the Ge only (x = 0) devices. The energy level of the dominant deep-level defect is observed to maintain a roughly fixed spacing relative to the conduction band edge in each device. As Sn concentration increases and the band gap decreases, this dominant defect energy level moves further from the mid-gap intrinsic Fermi level toward the valence band edge. This trend should equate to a beneficial reduction of trap-assisted recombination and generation rates in high Sn concentration devices. Notwithstanding this finding, theoretical considerations suggest the change in band structure (from direct to indirect bandgap) is likely most responsible for the increased displacement damage tolerance of the high Sn concentration devices.

Introduction

Silicon and germanium technology is pervasive for present day electronic applications, but the indirect energy gap of these two semiconductors generally prevents their use in photonic devices. Conventional mid-infrared photonic and optoelectronic materials based on III-V (e.g., gallium indium antimonide) and II-VI (e.g., mercury cadmium telluride) semiconductor alloys are generally incompatible with silicon-based integrated circuit processing, preventing monolithic integration of photonics for optical interconnects, etc., on a single integrated circuit chip [1]. Recent progress in $Ge_{1-x}Sn_x$ non-equilibrium growth techniques, with the demonstration of a direct energy gap for Sn concentrations around 7%, promises significant optical performance similar to the III-V and II-VI semiconductors, but compatible with the silicon complementary-metal-oxide-semiconductor (CMOS) device processing that dominates the semiconductor industry [2] [3]. If fabrication of reliable, high-quality Si- and Ge-based direct bandgap semiconductors can be realized, significant defense industrial base improvements are expected in areas including aircraft and satellite-based integrated circuits, infrared countermeasures, and chemical spectroscopy, with lower power consumption and higher speed than today's technology [4].

In order to realize the promise of these materials, however, native defects, impurities, and defect-impurity complexes must be better understood and controlled. Deep-level defects, in particular, decrease the radiative efficiency of photonic devices via Shockley-Read-Hall (SRH) non-radiative recombination of excess electron-hole pairs. Such defects are often associated with the displacement damage that accumulates in certain radiation environments. Much is known about defect properties in pure germanium, and some data have been published on defect properties in germanium-tin [5]–[7], but very little is known about the dependence of these properties on tin concentration. Furthermore, no studies of radiation effects on GeSn-based light emitting devices have been reported to date, so the questions about tin concentration dependencies extend to the device level operation as well. The present study seeks to answer such questions with a view toward the use of GeSn-based photonic and optoelectronic devices on Earth-orbiting satellites.

This work was sponsored by the Air Force Office of Scientific Research (11767875-AFIT and FA9550–17–1–0314-ASU).

Experiment

The $Ge_{1-x}Sn_x$-based light emitting diodes (LEDs) used in this study were fabricated at Arizona State University [8], [9]. The devices were grown by chemical vapor deposition (CVD) on Si (100) using ultra-low temperature deposition of highly reactive Ge and Sn hydrides. Active device areas were defined in circular mesas 360 µm and 580 µm in diameter and Cr/Au metallization was deposited for ohmic contacts to the p^+ and n^+ regions (Fig. 1), doped with 2×10^{19} cm^{-3} boron and phosphorous atoms, respectively. The Sn concentration, *y*, in the p^+ region is slightly lower than the Sn concentration, *x*, in the intrinsic region to improve light extraction and promote carrier confinement in the intrinsic region. A thin passivation layer of SiO_2 was deposited on the outer surfaces of the device mesa.

The intrinsic regions of these devices are unintentionally doped at levels around 10^{16}-10^{17} cm^{-3}, with the germanium ($x = 0$) sample being n-type and the $x > 0$ samples being p-type. The properties of the intrinsic regions of these devices are listed in Table 1. The carrier concentrations were estimated based on capacitance-voltage (C-V) measurements, and the part of the intrinsic region probed by standard deep-level transient spectroscopy (DLTS) pulse/measurement bias parameters was also estimated from the C-V data.

Electroluminescence (EL) intensity, current-voltage (I-V), C-V, and DLTS characterization data were collected before and after 2 MeV proton irradiation. This was followed by isochronal annealing for 30 minutes at 120 °C and 200 °C to explore the thermal stability of the radiation-induced deep-level defects and device EL.

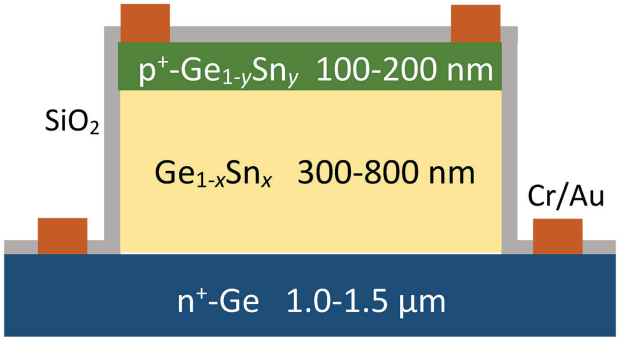

Figure 1. Schematic of device layers. Structural support is provided by a resistive silicon wafer substrate. The width of the actual device's mesa was about 1,000 times greater than the thickness.

Table 1. Device intrinsic region properties.

Sn Conc. [mol. %]	Carrier Conc./ type [cm^{-3}]	Thickness [nm]	Strain [%] "-/+" compress / tensile	Bandgap at 300 K [eV]
0.0	5×10^{16} n-type	790	+ 0.11	0.66
2.0 ± 0.1	2×10^{16} p-type	530	- 0.14	0.62
5.3 ± 0.1	1×10^{17} p-type	440	- 0.16	0.57
6.9 ± 0.1	2×10^{17} p-type	400	- 0.22	0.54
9.4 ± 0.1	2×10^{17} p-type	300	-0.32	0.46

EL intensity was measured at room temperature using a thermoelectrically cooled InGaAs detector, coupled to the test device through a low hydroxyl silica fiber bundle terminated in air within 1 millimeter of the face of the device. The wavelength range of the detector is 900–2570 nm, and the 1 meter fiber bundle transmits 400–2400 nm light with negligible attenuation. The EL from these devices was previously observed to fall within the range of 1400–2400 nm, with peak intensities at approximately 1600, 1700, 2100, and 2300 nm for Sn concentrations of 0%, 2%, 6.9%, and 9.4%, respectively [9]. Current was sourced through the devices in 3 ms pulses at an 18% duty cycle in increasing magnitude steps up to a current level corresponding to a 3.0 V applied bias. A reference signal was split off from the pulser to a lock-in amplifier to reduce noise in the photodetection voltage signal. Using this voltage signal as a relative measure of EL intensity, the relative radiation-induced degradation in this intensity, ΔEL, was quantified as

$$\Delta EL = -\frac{(Post\text{-}rad\ EL\ Signal)-(Pre\text{-}rad\ EL\ Signal)}{(Pre\text{-}rad\ EL\ Signal)} \times 100\%, \quad (1)$$

where the minus sign is included in front of the ratio to show degradation in EL as a positive quantity.

Temperature-dependent electrical characterization was performed from 24 to 296 K using a Semetrol DLTS, C-V, and I-V characterization system. DLTS measurements were performed both in the conventional fashion and in

JOURNAL OF RADIATION EFFECTS,
Research and Engineering
Vol. 38, No. 1, March 2020

current injection mode for detection of dominant majority carrier traps and minority carrier traps, respectively.

Stopping and range of ions in matter (SRIM) [10] Monte-Carlo simulations of the proton-target interactions were used to confirm that energy was deposited uniformly throughout the device intrinsic regions and to calculate the initial (instantaneous) vacancy concentration produced per unit proton fluence in each device. These simulations show that approximately 0.13 vacancies/μm/proton are deposited uniformly in the intrinsic region of each device, with only 5% fewer displacements in the 9.4% Sn devices due to reduced energy transfer to the higher mass Sn target atoms as compared to the lower mass Ge atoms. Thus, the amount of initial displacement damage per unit fluence is approximately the same in each device.

The beam current was selected to ensure devices remained within a few degrees of room temperature throughout the irradiation. Proton fluences up to 4×10^{14} cm^{-2} were applied over a period of 5–20 minutes, and the devices were then placed in liquid nitrogen storage to ensure they were subjected to no more than 1.5 hours of room temperature annealing prior to the first post-rad EL measurements.

Results and Discussion

EL intensity was measured on a total of 41 devices. Fig. 2 shows EL intensity as a function of applied current for devices before and after 4×10^{13} cm^{-2} irradiation. At this fluence level, little change is observed in the basic electrical characteristics of each device, such as the room temperature carrier concentration and the applied current at which EL intensity plateaus. Nevertheless, a clear degradation of the maximum EL intensity is apparent in all but one of the devices, and the greatest degradation is seen in the samples with the lowest tin concentration. Fig. 3 summarizes this trend, including the results at higher fluence levels. As indicated by the 95% confidence interval error bars, there was considerable variability in the ΔEL results, reflecting a combination of measurement uncertainty and material variations in different devices from the same sample. Nevertheless, the high Sn concentration devices clearly exhibit less degradation than the low Sn concentration devices. For the devices irradiated at 4×10^{13} cm^{-2}, the average degradation of the 0% Sn and 9.4% Sn devices was 47.7% ± 5.8% and 4.7% ± 5.1%, respectively.

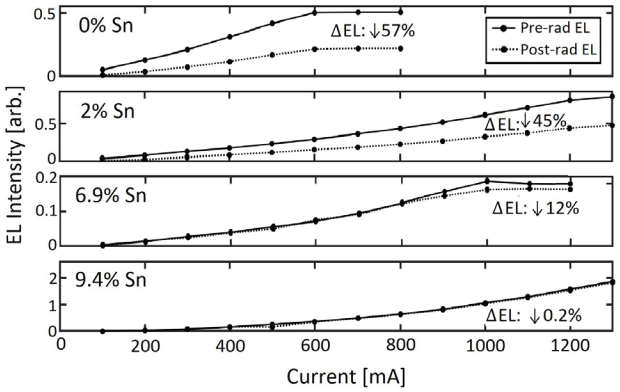

Figure 2. EL intensity versus applied current before and after 4×10^{13} cm^{-2} irradiation.

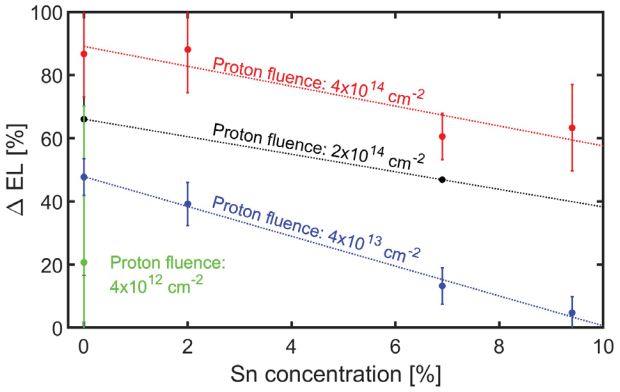

Figure 3. Dependence of EL intensity degradation (ΔEL) on Sn concentration and proton fluence. Each point is an average of up to six devices, and the error bars reflect a 95% confidence interval for the ΔEL measurement. Each black point reflects measurement of a single device.

Prior to irradiation, DLTS rate window signal levels were generally below 10^{-3} Δ*C*/*C*, with associated deep-level defect concentrations up to 5×10^{14} cm^{-3} in the devices of higher Sn concentration and no more than 1×10^{13} cm^{-3} in the 0% and 2% Sn devices. Electron trapping generally dominated the as-grown and 4×10^{13} cm^{-2} fluence post-rad DLTS spectra under standard and injection pulse/measurement bias parameters. Following 4×10^{14} cm^{-2} proton irradiation, however, hole trapping clearly dominated over electron trapping, and the representative DLTS spectra are shown in Fig. 4 (see next page). In this figure, 545 s^{-1} rate windows are shown for 0%, 2%, and 6.9% Sn devices. Hole traps are observed as majority carrier traps (yielding a negative capacitance transient) in the 2.0–6.9% Sn devices, and as minority carrier traps (yielding a positive capacitance transient) in the 0% Sn device. All the observed peaks overlap to greater or lesser degree with adjacent peaks, so a Gaussian peak fitting method was used

to infer the individual peak temperatures and magnitudes. These fitting results showed consistency at different rate windows and dozens of different DLTS data sets for each device. A dominant, thermally stable hole trap, labeled H1, was observed in each of the devices.

Based on the measured DLTS parameters and thermal stability, as well as consideration of likely impurities in these devices, this hole-trap can be attributed to the (-/0) transition of the V_{Ge}-P complex [11]. In the 0% Sn devices, this peak was not initially dominant, but it increased in magnitude with isochronal annealing up to 110 °C. This was one of several instances in which the V_{Ge}-P complex appeared to grow in magnitude at elevated temperatures, presumably as additional V_{Ge} were released from less stable defect complexes. In the 0% and 2% Sn samples, this H1 peak was little affected by neighboring peaks, and the apparent activation energy, E_{V-P}, was readily deduced from Arrhenius plot fitting. In the devices with higher Sn concentration, the Arrhenius plot fitting technique was applied to the H1 peak that resulted from a 2 or 3 Gaussian peak deconvolution algorithm in the Semetrol analysis software. This procedure entailed greater uncertainty in the extracted values of E_{V-P} for the higher Sn concentration samples. These extracted DLTS parameters are shown in Table 2 for devices at five different Sn concentration levels, including one at 5.3% Sn, which was not available for the EL measurements.

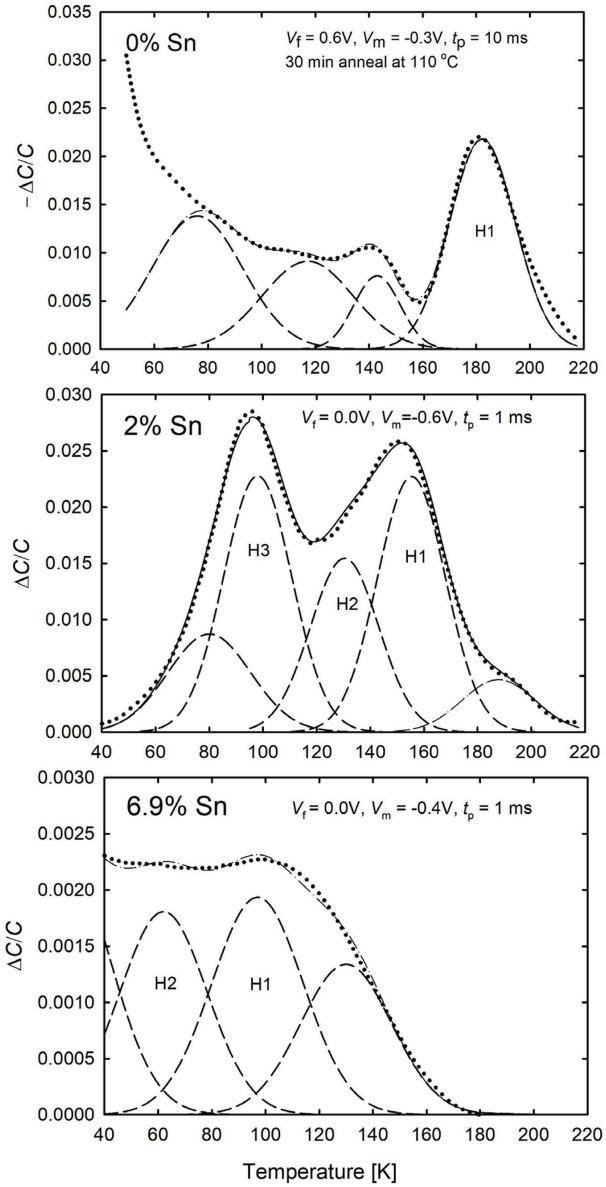

Figure 4. DLTS spectra (545 s^{-1} rate window) of hole traps following 4x10^{14} cm^{-2} proton fluence. The 0% Sn spectrum reflects minority carrier trapping obtained by injection DLTS measurement after annealing at 110 °C for 30 minutes.

Table 2. Measured DLTS parameters of dominant hole traps. The capture cross sections inferred from Arrhenius fitting were on the order of 10^{-13} cm^2, but the associated uncertainties were generally too large to support meaningful comparisons.

Sn Conc. [%]	Defect Label	T_{peak} [K]	E_T [eV]	Defect Attribution
0	H1	180	0.35 ± 0.02	V_{Ge}-P
2.0	H1	155	0.31 ± 0.02	V_{Ge}-P
	H2	130	0.19 ± 0.03	-
	H3	98	0.14 ± 0.01	V_{Ge}-Sn
5.3	H1	106	0.21 ± 0.03	V_{Ge}-P
	H2	72	-	-
	H3	38	-	V_{Ge}-Sn
6.9	H1	97	0.18 ± 0.03	V_{Ge}-P
	H2	62	-	-
9.4	H1	86	0.13 ± 0.03	V_{Ge}-P
	H2	-	-	-

In the 2% Sn devices, a prominent hole trap peak, labeled H3, was clearly discernible, and this peak also appeared to be present (though less clearly) in the 5.3%, 6.9%, and 9.4% devices. Based on the measured DLTS parameters, thermal stability, and the absence of this peak in the 0% Sn devices, this hole-trap can be attributed to the (2-/-) transition of the V_{Ge}-Sn complex, which was previously only reported for germanium doped with tin [12]. The V_{Ge}-Sn complex is found to be less thermally stable than the V_{Ge}-P complex, and in several instances the V_{Ge}-P complex was observed to increase in concentration during 120 °C annealing, presumably as germanium vacancies dissociated from tin impurities. The peaks labeled "H2" and the unlabeled peaks in these spectra are unidentified at present, but there is some evidence that the peaks to the left of H1 on the temperature scale of the 0% Sn devices are not of the same origin as H2 and H3 in the other devices.

These DLTS results are suggestive of one potential mechanism for the lower luminescence intensity degradation in the high Sn concentration devices. Trap-assisted SRH recombination of excess electrons and holes is a non-radiative process in which the carrier energy is given up through atomic lattice collisions (i.e., phonons) rather than photon emission. The net rate of SRH recombination (or generation, if carrier concentrations are below equilibrium levels) is given by (2) [13]. Here, n_i is the intrinsic carrier concentration, n and p are the non-equilibrium carrier concentrations (under the applied forward bias in this case), and E_T and E_i are the trap and intrinsic energy levels referenced to the valence band edge. The mean lifetimes of the electrons and holes, denoted by τ_n and τ_p, respectively are determined by the trap concentration and capture cross sections, as well as the thermal velocities of the carriers.

$$\left.\frac{\partial p}{\partial t}\right|_{R-G} = \left.\frac{\partial n}{\partial t}\right|_{R-G} = \frac{n_i^2 - np}{\tau_p(n + n_1) + \tau_n(p + p_1)} \quad (2)$$

$$n_1 \equiv n_i e^{(E_T - E_i)/kT}$$

$$p_1 \equiv n_i e^{(E_i - E_T)/kT}$$

According to (2), the SRH recombination or generation rate is maximized when E_T is equal to E_i. If n_i is large compared to both n and p (e.g., in the intrinsic region under reverse bias), the SRH recombination rate decreases exponentially as $|E_i - E_T|$ increases. However, in the forward-biased operation of typical LEDs, n and p are large compared to n_i, so a strong dependence on $|E_i - E_T|$ is not expected. In this regime, it is likely of greatest significance that the 6.9% and 9.4% Sn devices are near or beyond the indirect/direct bandgap transition point. Direct bandgap semiconductors should be inherently less sensitive to increases in deep-level defect concentrations due to the greater number of electrons in the Γ valley of the conduction band, which readily recombine with holes in radiative transitions. At lower injection levels, $|E_i - E_T|$ can be a significant factor, but the numerous other dependencies in (2) put theoretical prediction of the SRH rates outside the scope of this work at present.

In Fig. 5 the energy levels for the dominant H1 hole trap, E_{H1}, are shown relative to E_i at each Sn concentration. It is clear that $|E_i - E_{H1}|$ is relatively small in the 0% and 2% Sn devices and relatively large in the 5.3%, 6.9%, and 9.4% Sn devices. The bandgap energies decrease with Sn concentration, and the E_{H1} levels decrease to a greater extent than the corresponding E_i levels. In order to investigate this trend more closely, the change in E_{H1} was plotted versus the change in bandgap at the indirect (L) and direct (Γ) points in momentum space. Fig. 6 (see next page) shows these energy level changes

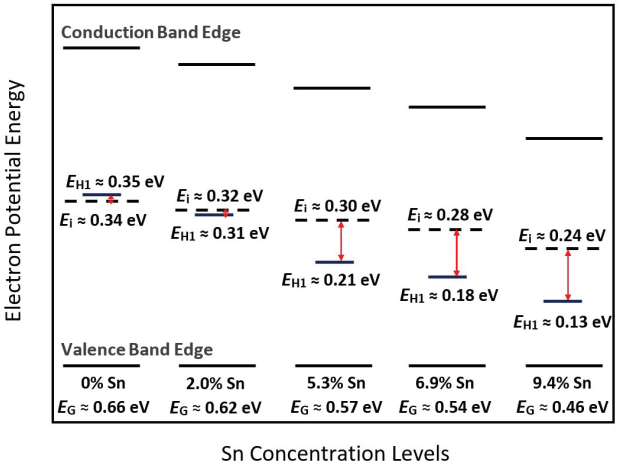

Figure 5. Proximity of H1 hole trap energy level (E_{H1}) relative to the intrinsic Fermi energy level (E_i) for different Sn concentrations at 300 K. Above ~5% Sn, the H1 trap energy is relatively far removed from E_i.

compared to the 0% Sn values. It shows that the H1 level changes roughly as if pinned to the conduction band edge, with a slightly closer correspondence to the conduction band edge at the L point than at the Γ point. The trap energy level associated with the phosphorous-vacancy complex in SiGe was reported to show similar behavior [14].

If the SRH mechanism contributes to non-radiative recombination in forward-biased LEDs, it should also generate leakage current when these devices are operated under reverse bias as light detectors. The high Sn concentration devices presumed to have lower SRH recombination rates should also show lower SRH generation rates, and thus, exhibit lower radiation-induced leakage current. However, Fig. 7 shows that the radiation-induced increase in leakage current density (ΔJ_L) is greater in the high Sn concentration samples than in the low Sn concentration samples. The most likely explanation for this result is that a source of leakage current other than SRH generation in the intrinsic region volume is dominant, such as current related to charge trapping in the SiO_2 passivation layer (the total ionizing dose is 100s of Mrad). Specifically, the interface between the i and n^+ regions of the p-i-n structure is more defective in the as-grown devices with high Sn concentration due to lattice mismatch [9]. The field effect from holes trapped in the oxide might increase the extent of the depletion region in the vicinity of these interface defects and the sidewall surface states, thereby increasing the overall leakage current. The 0% Sn devices have a smaller lattice mismatch at the opposite interface (between the i and p^+ regions). Furthermore, the 0% Sn devices would be immune to this effect because the field from trapped holes would cause the majority carrier electrons to accumulate rather than become depleted in the i region, whereas the majority carrier holes in the GeSn devices would be depleted under this same field effect.

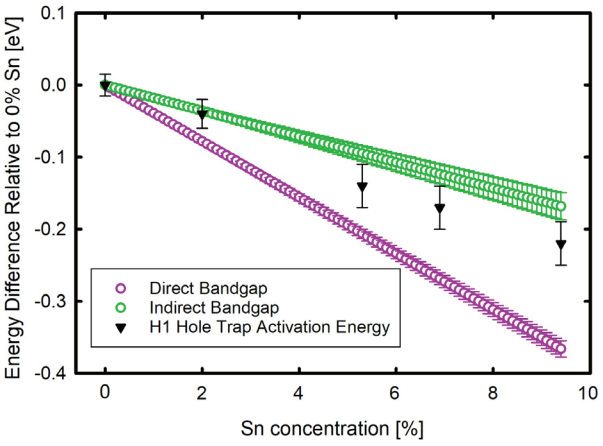

Figure 6. Change in direct and indirect bandgap energies and V_{Ge}-P activation energies in $Ge_{1-x}Sn_x$ as a function of Sn concentration relative to 0% Sn. The bandgap energies and associated error bars are taken from the empirical fit expressions in [15]. The H1 activation energies were measured by DLTS in this study.

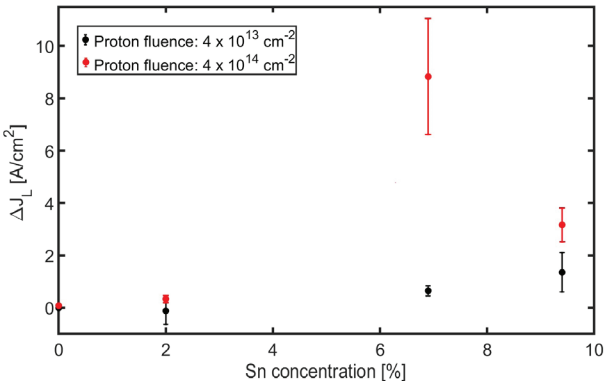

Figure 7. Dependence of radiation-induced change in leakage current density (ΔJ_L) on Sn concentration.

Conclusion

The main result of this research strongly suggests that $Ge_{1-x}Sn_x$ alloys with high Sn concentration are more resistant to luminescence degradation effects of displacement damage than their germanium counterparts. The EL experiments showed that $Ge_{1-x}Sn_x$ devices with higher Sn concentration were up to 10 times more resistant to proton displacement damage than the germanium (0% Sn) devices. DLTS measurements showed that the dominant radiation-induced deep-level carrier trap (presumed to be a V_{Ge}-P complex) has an energy level near E_i in the 0% and 2.0% Sn devices, but far from E_i in the 6.9% and 9.4% devices, thus offering a partial explanation for the higher rate of non-radiative recombination in the irradiated 0% and 2.0% Sn devices. While this mechanism is presumed to depend on the presence of phosphorus impurities, the result may also be expected to apply to $Ge_{1-x}Sn_x$ alloys containing other common group V impurities, such as As and Sb. As was noted, SRH theory suggests the trap energy levels of the dominant defects are unimportant compared to other factors when current injection levels are high.

Relatively high concentrations of radiation-induced atomic displacements were necessary to cause significant degradation in the EL intensity from these devices, suggesting such light emitting devices would be very tolerant to harsh space radiation environments over many years, regardless of Sn concentration. Detector devices based on these materials, however, could be less tolerant to trap-assisted generation current resulting from these same concentrations of defects. I-V measurement results showed that radiation-induced reverse-bias leakage current was up to 10 times greater in the high Sn devices than in the low Sn devices, presumably based on mechanisms other than SRH generation in the intrinsic region volume; such mechanisms may depend on the total ionizing dose as much as the displacement damage dose.

Acknowledgment

The authors would like to express their sincere appreciation to Dr. Gernot S. Pomrenke of the Air Force Office of Scientific Research for his support of this work (11767875-AFIT and FA9550-17-1-0314-ASU). Also, the excellent service provided by the staff of the Edwards Accelerator Laboratory at Ohio University was greatly appreciated.

References

[1] R. Soref, "Mid-infrared photonics in silicon and germanium," *Nat. Photonics*, vol. 4, p. 495, 2010.

[2] S. Zaima *et al.*, "Growth and application of GeSn-related group-IV semiconductor materials," *Sci. Technol. Advanced Materials*, vol. 16, p. 043502, 2015.

[3] E. Kasper, M. Kittler, M. Oehme, and T. Arguirov, "Germanium tin: silicon photonics toward the mid-infrared," *Photonics Res.*, vol. 1, no. 2, p. 69, 2013.

[4] "AFOSR STTR Topic AF16-AT28," Dec. 2015. [Online]. Available: https://www.sbir.gov/sbirsearch/detail/871843. [Accessed 24 Sept. 2018].

[5] B. Wang *et al.*, "Electrical characterization and deep-level transient spectroscopy of $Ge_{0.873}Si_{0.104}Sn_{0.023}$ photodiode grown on Ge platform by ultra-high vacuum chemical vapor deposition," *Thin Solid Films*, vol. 654, p. 77, 2018.

[6] S. Gupta *et al.*, "Electrical properties of extended defects in strain relaxed GeSn," *Appl. Physics Lett.*, vol. 113, p. 022102, 2018.

[7] M.-Y. Ryu *et al.*, "Degenerate parallel conducting layer and conductivity type conversion observed from p-$Ge_{1-y}Sn_y$ (y = 0.06%) grown on n-Si substrate," *Appl. Physics Lett.*, vol. 101, p. 131110, 2012.

[8] J. Gallagher *et al.*, "Electroluminescence from GeSn heterostructure pin diodes at the indirect to direct transition," *Appl. Physics Lett.*, vol. 106, p. 091103, 2015.

[9] J. Gallagher *et al.*, "Non-radiative recombination in $Ge_{1-y}Sn_y$ light emitting diodes: The role of strain relaxation in tuned heterostructure designs," *J. Appl. Physics*, vol. 117, p. 245704, 2015.

[10] J.F. Ziegler, J.P. Biersack, and M.D. Ziegler, *SRIM: The Stopping and Range of Ions in Matter*, Morrisville, NC: Lulu Press Co., 2015.

[11] V. Markevich *et al.*, "Vacancy-goup-V-impurity atom pairs in Ge crystals doped with P, As, Sb, and Bi," *Physical Rev. B*, vol. 70, p. 235213, 2004.

[12] V. Markevich *et al.*, "Tin-vacancy complex in germanium," *J. Appl. Physics*, vol. 109, p. 083705, 2011.

[13] R.F. Pierret, *Semiconductor Device Fundamentals*, Reading, MA: Addison-Wesley, 1996.

[14] M. Mamor, M. Elzain, K. Bouziane, and S.H. Al Harthi, "Deep-level transient spectroscopy study of the E center in n-Si and partially relaxed n-$Si_{0.9}Ge_{0.1}$ alloy layers," *Physical Rev. B*, vol. 77, p. 035213, 2008.

[15] L. Jiang *et al.*, "Compositional dependence of the direct and indirect band gaps in $Ge_{1-y}Sn_y$ alloys from room temperature photoluminescence," *Semiconductor Sci. Technol.*, vol. 29, p. 115028, 2014.